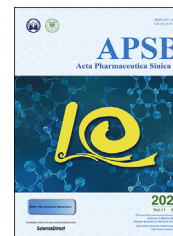




Chinese Pharmaceutical Association
Institute of Materia Medica, Chinese Academy of Medical Sciences

Acta Pharmaceutica Sinica B

www.elsevier.com/locate/apsb
www.sciencedirect.com



ORIGINAL ARTICLE

Can remdesivir and its parent nucleoside GS-441524 be potential oral drugs? An *in vitro* and *in vivo* DMPK assessment



Jiashu Xie*, Zhengqiang Wang*

Center for Drug Design, College of Pharmacy, University of Minnesota, Minneapolis, MN 55455, USA

Received 5 February 2021; received in revised form 28 February 2021; accepted 5 March 2021

KEY WORDS

Remdesivir;
GS-441524;
COVID-19;
SARS-CoV-2;
Nucleoside;
Antiviral;
Oral bioavailability;
Drug metabolism

Abstract Remdesivir (RDV) is the only US Food and Drug Administration (FDA)-approved drug for treating COVID-19. However, RDV can only be given by intravenous route, and there is a pressing medical need for oral antivirals. Significant evidence suggests that the role of the parent nucleoside GS-441524 in the clinical outcomes of RDV could be largely underestimated. We performed an *in vitro* and *in vivo* drug metabolism and pharmacokinetics (DMPK) assessment to examine the potential of RDV, and particularly GS-441524, as oral drugs. In our *in vitro* assessments, RDV exhibited prohibitively low stability in human liver microsomes (HLMs, $t_{1/2} = \sim 1$ min), with the primary CYP-mediated metabolism being the mono-oxidation likely on the phosphoramidate moiety. This observation is poorly aligned with any potential oral use of RDV, though in the presence of cobicistat, the microsomal stability was drastically boosted to the level observed without enzyme cofactor NADPH. Conversely, GS-441524 showed excellent metabolic stability in human plasma and HLMs. In further *in vivo* studies in CD-1 mice, GS-441524 displayed a favorable oral bioavailability of 57%. Importantly, GS-441524 produced adequate drug exposure in the mice plasma and lung, and was effectively converted to the active triphosphate, suggesting that it could be a promising oral antiviral drug for treating COVID-19.

© 2021 Chinese Pharmaceutical Association and Institute of Materia Medica, Chinese Academy of Medical Sciences. Production and hosting by Elsevier B.V. This is an open access article under the CC BY-NC-ND license (<http://creativecommons.org/licenses/by-nc-nd/4.0/>).

Abbreviations: ADK, adenosine kinase; Cobi, cobicistat; CYP, cytochrome P450; DMPK, drug metabolism and pharmacokinetics; EMS, enhanced mass scan; EPI, enhanced product ion; FIPV, feline infectious peritonitis coronavirus; HINTs, histidine triad nucleotide binding proteins; HLMs, human liver microsomes; IDA, information dependent acquisition; MLMs, mouse liver microsomes; MRM, multiple reaction monitoring; RdRp, RNA-dependent RNA-polymerases; RDV, remdesivir; SOF, sofosbuvir; TAF, tenofovir alafenamide.

*Corresponding authors. Tel.: +1 612 6242945 (Jiashu Xie), +1 612 6267025 (Zhengqiang Wang).

E-mail addresses: jxie@umn.edu (Jiashu Xie), wangx472@umn.edu (Zhengqiang Wang).

Peer review under responsibility of Chinese Pharmaceutical Association and Institute of Materia Medica, Chinese Academy of Medical Sciences.

<https://doi.org/10.1016/j.apsb.2021.03.028>

2211-3835 © 2021 Chinese Pharmaceutical Association and Institute of Materia Medica, Chinese Academy of Medical Sciences. Production and hosting by Elsevier B.V. This is an open access article under the CC BY-NC-ND license (<http://creativecommons.org/licenses/by-nc-nd/4.0/>).

1. Introduction

The severe acute respiratory syndrome coronavirus 2 (SARS-CoV-2) is the causative agent for the ongoing coronavirus disease 2019 (COVID-19) pandemic, which to date has resulted in more than 113 million confirmed cases and over 2.5 million deaths worldwide according to the World Health Organization¹. SARS-CoV-2, an enveloped positive-sense single-stranded RNA virus belonging to the broad and highly diverse family of coronavirus², is highly contagious ($R_0 > 2.2$)^{3,4}, and transmitted primarily through the respiratory route by droplets, airborne or direct contact^{5,6}. A number of epidemiological studies have shown that transmission can occur from asymptomatic or presymptomatic patients^{7–10}, with peak viral load observed at the time of symptom onset or in the first week of illness^{6,11–15}. Importantly, SARS-CoV-2 viral load is strongly associated with the disease severity and mortality^{14,16}. Therefore, an antiviral treatment administered shortly after the infection would have maximal benefits by inhibiting viral replication, interrupting the transmission chain, and more importantly, preventing disease progression to severe or critical stages¹⁷. Currently, RDV (Fig. 1) is the only antiviral drug approved by the FDA for the treatment of COVID-19¹⁸. Initially developed as an antiviral to treat Ebola virus infections^{19–21}, RDV exhibited broad-spectrum antiviral activity against a panel of RNA viruses including SARS-CoV, Middle East respiratory syndrome coronavirus and SARS-CoV-2^{22–27}. However, RDV is authorized to be administered by intravenous (iv) infusion only in inpatient settings²⁸. Early antiviral treatment calls for drug regimens that can be self-administered, *e.g.*, oral drugs, which would be particularly beneficial for post exposure prophylaxis.

RDV is a nucleotide prodrug (ProTide) of the parent 1'-cyano substituted adenosine C-nucleoside (GS-441524, Fig. 1)²¹. The potency of RDV hinges on its intracellular conversion into GS-441524 triphosphate, the pharmacologically active metabolite GS-443902 (Fig. 1), which competes against the endogenous ATP for recognition and incorporation by the viral RNA-dependent RNA-polymerases (RdRp)^{23,29,30}. Structurally, RDV features a chemically installed monophosphate to bypass the rate-limiting, kinase-mediated intracellular monophosphorylation. Such a design is presumably necessitated by insufficient intracellular bioactivation of the parent nucleoside. However, a few lines of evidence strongly indicate that kinase bypass may not be required and that the parent nucleoside may be sufficiently converted to the active triphosphate. First, GS-441524 demonstrated a similar potency to RDV in inhibiting SARS-CoV-2 replication in established Calu-3 2B4 human lung adenocarcinoma cells²³. Second, in Vero E6 cells, GS-441524 yielded the triphosphate (GS-443902) at a level 3.5-fold higher than that of RDV, corresponding to higher anti-SARS-CoV-2 potency²³. Third, GS-441524 has been proven highly efficacious and well tolerated in cats against feline infectious peritonitis coronavirus (FIPV)^{31–33}. Notably, following iv or subcutaneous administration of GS-441524 (5 mg/kg) to cats, the triphosphate (GS-443902) in peripheral blood mononuclear cells maintained for over 24 h at levels 8–20-fold higher than its *in vitro* EC₅₀ (0.78 $\mu\text{mol/L}$) against FIPV³³. Lastly, RDV was found to exist predominantly as GS-441524 in systemic blood circulation following iv administration^{19,30,34–36}. RDV exhibited a short plasma half-life ($t_{1/2}$) of about 1 h following iv infusion in phase I clinical studies whereas the predominant GS-441524 metabolite persisted in the circulation with a $t_{1/2}$ of about 27 h³⁰. Collectively,

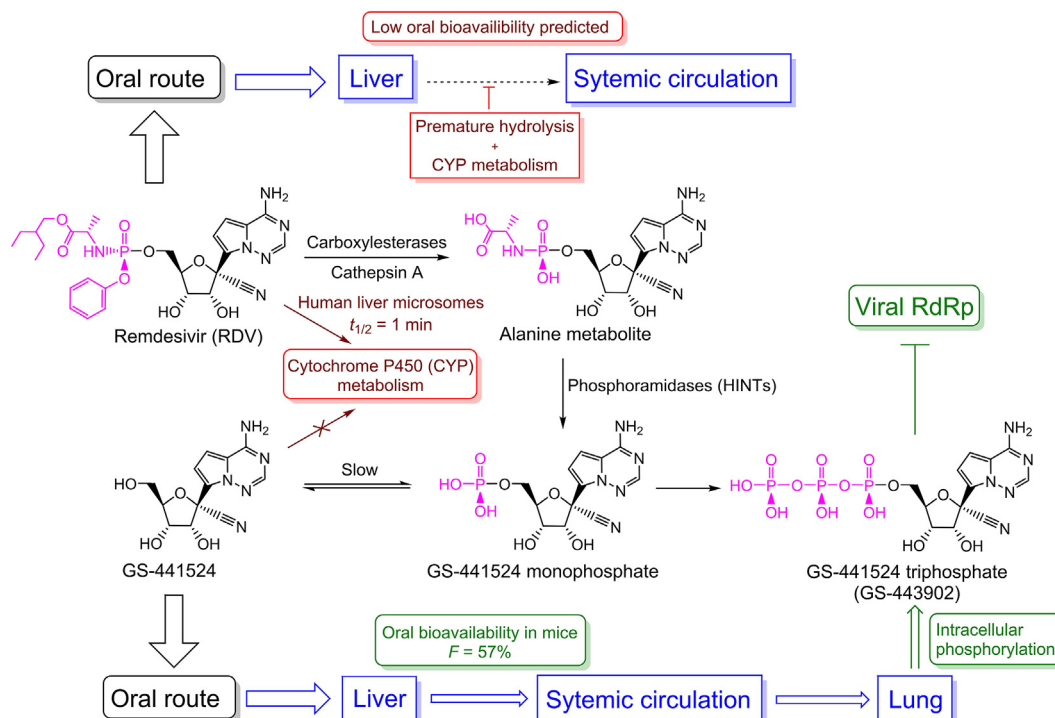


Figure 1 Structures, mechanisms of activation and action, and potential dispositions of RDV and GS-441524 following oral administration.

these observations imply that the contribution of GS-441524 to the clinical outcomes of RDV may be largely underestimated. In addition, while RDV is a substrate for the CYP 2C8, 2D6 and 3A4^{28,37}, GS441524 is not for any major CYP enzymes including 1A1, 1A2, 2B6, 2C8, 2C9, 2C19, 2D6, 3A4, or 3A5²⁸, suggesting that GS-441524 may not suffer from excessive hepatic extraction. Taken together, one could argue that GS-441524 might have advantages over RDV for COVID-19 treatment³⁴. Given the urgent need for an oral antiviral against COVID-19 and the clinical efficacy of RDV, we evaluated the potential of GS-441524 for oral use by performing a DMPK assessment *in vitro* and *in vivo*. We also performed the *in vitro* metabolic and metabolite profiling assays on RDV as details on the CYP-mediated hepatic clearance have not been fully disclosed or characterized²⁸. Such studies could provide valuable information to guide future medicinal chemistry design and selection of oral nucleoside prodrugs.

2. Materials and methods

2.1. Materials

RDV (catalog No. 329511) and GS-441524 (catalog No. 555299) were purchased from MedKoo Biosciences, Inc (Morrisville, NC, USA). The active triphosphate metabolite (GS-443902, catalog No. HY-126303) and cobicistat (catalog No. HY-10493) were purchased from MedChemExpress (Monmouth Junction, NJ, USA). Nicotinamide adenine dinucleotide phosphate (NADPH, catalog No. D00145545) was purchased from EMD Millipore Calbiochem (Darmstadt, Germany). Human liver microsomes (HLMs, catalog No. H2620) and CD-1 mice liver microsomes (MLMs, catalog No. M1000) were purchased from Sekisui XenoTech (Kansas City, KS, USA). Pooled CD-1 mice plasma (catalog No. IGMSCD1PLAK2E100ML) and human plasma (catalog No. IPLALIH100ML) were purchased from Innovative Research (Novi, MI, USA). LC/MS grade water (catalog No. W6-4), acetonitrile (catalog No. A955-4) and formic acid (catalog No. A117-50) were purchased from Fisher Chemical (Fair Lawn, NJ, USA).

2.2. *In vitro* metabolic assessment

The metabolic stability of RDV and GS-441524 were assessed *in vitro* in human and mouse plasma, and in liver microsomes. The plasma stability assay was performed in duplicate by incubating each compound (1 $\mu\text{mol/L}$ final concentration) in diluted mouse and human plasma (80% in 0.1 mol/L potassium phosphate buffer, pH 7.4) at 37 °C. At 0, 1, 3, 6, and 24 h, a 50 μL aliquots of the plasma mixture were taken and quenched with 150 μL of acetonitrile containing 0.1% of formic acid. The quenched samples were vortexed and centrifuged at 15,000 rpm (Eppendorf centrifuge 5424 R, Enfield, CT, USA) for 5 min at 4 °C. The supernatants were collected and analyzed by LC/MS/MS to determine the *in vitro* plasma $t_{1/2}$.

The microsomal stability assay was performed using commercially available human and mouse liver microsomes. Briefly, each compound (1 $\mu\text{mol/L}$ final concentration) was incubated in a 0.1 mol/L potassium phosphate buffer solution (pH 7.4, 37 °C) containing liver microsomal protein (0.5 mg/mL final

concentration), the enzyme cofactor NADPH (1 mmol/L final concentration) and MgCl_2 (1 mmol/L final concentration). The reaction was initiated by the addition of the tested compound. For incubation with the CYP3A inhibitor, cobicistat was pre-incubated in the microsomal system for 5 min before the addition of the test compound. A negative control without NADPH was also performed in parallel to assess any chemical instability or non-NADPH dependent enzymatic degradation. All reactions were carried out at least in duplicate with independent assays. A 50 μL of reaction mixture was taken at different time points (0, 5, 15, 30, and 60 min), and quenched with 150 μL of acetonitrile containing 0.1% of formic acid. The samples were then vortexed and centrifuged at 15,000 rpm for 5 min at 4 °C. The supernatants were collected and analyzed by LC/MS/MS to determine the *in vitro* metabolic $t_{1/2}$ and intrinsic clearance (CL_{int}).

2.3. *In vivo* pharmacokinetic profiling in mice

The following mice pharmacokinetic studies were approved by the Institutional Animal Care and Use Committee (IACUC protocol ID. 1811–36511 A) at the University of Minnesota and the experiments were conducted in compliance with IACUC policies and internal animal welfare guidelines. CD-1 mice (strain code: 022) were purchased from Charles River Laboratories (Wilmington, MA, USA), and were accommodated and cared by the AAALAC-certified Research Animal Resources facility in the University of Minnesota, USA.

Oral bioavailability of GS-441524 was evaluated in 8-week-old male CD-1 mice *via* two administration routes: tail vein iv injection (5 mg/kg) and oral gavage (*po*, 10 mg/kg), 4 mice per route. GS-441524 was dissolved in Dulbecco's phosphate-buffered saline containing 30% PEG-300 at a concentration of 4 mg/mL (1% DMSO). Blood samples ($\sim 20 \mu\text{L}$ /time point) were collected into EDTA-fortified tubes serially by saphenous vein puncture at 5, 15, 30 min and 1, 2, 4, 8, 24 h. The samples were then centrifuged at 3000 rpm for 10 min at 4 °C to obtain plasma. Plasma concentrations were determined by LC/MS/MS, and the concentration–time data were analyzed using Phoenix WinNonlin (v8.1, Pharsight Corporation, Mountain View, CA, USA) with non-compartmental modeling. Oral bioavailability ($F\%$) was determined by comparing the area under the curve (AUC) of the oral and iv administration routes as Eq. (1):

$$F(\%) = (\text{AUC}_{\text{po}} / \text{AUC}_{\text{iv}}) \times (\text{Dose}_{\text{iv}} / \text{Dose}_{\text{po}}) \quad (1)$$

Tissue distribution of GS-441524 and its final active triphosphorylated metabolite (GS-443902) were determined in nine male CD-1 mice after oral dosing (20 mg/kg). At 1, 2 and 4 h post-dosing, three mice per time point were euthanized and liver and lung tissues were collected and snap frozen on dry ice. Blood samples were also collected into EDTA-fortified tubes and plasma were obtained by centrifuged at 3000 rpm for 10 min at 4 °C. All plasma and tissue samples were stored in a $-80 \text{ }^\circ\text{C}$ freezer until LC/MS/MS analysis.

2.4. LC/MS/MS instrumentation

Quantitation and analysis of RDV, GS-441524, and their metabolites were carried out on a system consisting of an Agilent 1260 Infinity HPLC (Agilent Technologies, Santa Clara, CA, USA) and

an AB Sciex QTrap 5500 mass spectrometer (AB Sciex LLC, Toronto, Canada).

2.5. Determination of RDV and its metabolites

For RDV, chromatographic separation was achieved on a Phenomenex Kinetex C18 column (50 mm × 2.1 mm, 2.6 μm). The two eluents were 0.1% formic acid in water (A) and 0.1% formic acid in acetonitrile (B). The mobile phase was delivered at a flow rate of 0.5 mL/min using a gradient of A and B as follows: from 0 to 1 min, 5% to 90% (v/v) B; from 1 to 2.8 min, 90% (v/v) B; from 2.8 to 3 min, 90% to 5% (v/v) B; from 3 to 6 min, 5% (v/v) B. RDV was detected by positive electrospray ionization (ESI) ion source with multiple reaction monitoring (MRM) transitions of m/z 603.3 to 402.3 and m/z 603.3 to 318.2. For the alanine metabolite (Ala-met) and mono-oxidation metabolite, chromatographic separation was achieved on a Thermo Aquasil C18 column (150 mm × 2.1 mm, 2.6 μm). Same eluents were used as in the determination of RDV. The mobile phase was delivered at a flow rate of 0.3 mL/min using a gradient of A and B as follows: from 0 to 1.5 min, 3% to 90% (v/v) B; from 1.5 to 3.8 min, 90% (v/v) B; from 3.8 to 4 min, 90% to 3% (v/v) B; from 4 to 7.5 min, 3% (v/v) B. The Ala-met and mono-oxidation metabolite were detected by ESI ion source with fast polarity switch and MRM transitions of m/z 441.1 to 150.0 and m/z 619.3 to 200.1, respectively.

2.6. Quantitation of GS-441524 in mice plasma

An aliquot of 10 μL of each thawed plasma sample was treated with 70 μL of acetonitrile containing 0.1% formic acid and DMSO mixture (6:1, v/v). The samples were vortexed and centrifuged at 15,000 rpm for 5 min at 4 °C. A 1 μL aliquot of the supernatant of each sample was injected into the LC/MS/MS for analysis. Chromatographic separation was achieved on a Phenomenex Kinetex C18 column (50 mm × 2.1 mm, 2.6 μm). The two eluents were 5 mmol/L ammonium formate in water (A) and 0.1% formic acid in acetonitrile (B). The mobile phase was delivered at a flow rate of 0.5 mL/min using a gradient of A and B as follows: from 0 to 1.5 min, 3% to 80% (v/v) B; from 1.5 to 2.8 min, 80% (v/v) B; from 2.8 to 3 min, 80% to 3% (v/v) B; from 3 to 6.5 min, 3% (v/v) B. GS-441524 was detected by positive ESI with MRM transitions of m/z 292.1 to 202.1 and m/z 292.1 to 147.1. Concentrations of GS-441524 was determined using matrix-matched calibration curve prepared in blank CD-1 mouse plasma and quality samples were run in the middle and the end of the run to ensure accuracy and precision within 20%.

2.7. Quantitation of GS-441524 and GS-443902 in mice tissue homogenates

The frozen tissue samples were individually weighed and homogenized with 2- or 4-times equivalent volumes of eluent A as follows. An aliquot of 100 μL of each tissue sample was treated with 100 μL of methanol, DMSO and H₂O mixture (8:1:1, v/v/v) containing 500 nmol/L 5-iodo-dCTP as internal standard. The samples were frozen at -80 °C for 60 min followed by heated at 75 °C for 5 min. After centrifugation at 15,000 rpm for 15 min at 4 °C, a 2 μL aliquot of the supernatant of each sample was injected into the LC/MS/MS for analysis. Chromatographic

separation of analytes was achieved on a Waters XTerra MS C18 column (150 mm × 2.1 mm, 3.5 μm). The two eluents were 0.5% diethylamine in water, with the pH adjusted to 10 with acetic acid (A), and 50% acetonitrile in water (B). The mobile phase was delivered at a flow rate of 0.25 mL/min using a gradient of A and B as follows: from 0 to 4 min, 0 to 15% (v/v) B; from 4 to 4.5 min, 15% to 90% (v/v) B; from 4.5 to 7.5 min, 90% (v/v) B; from 7.5 to 8 min, 90% to 0% (v/v) B; from 8 to 15 min, 0% (v/v) B. GS-441524, GS-443902 and the internal standard 5-iodo-dCTP were detected by negative ESI with MRM transitions of m/z 290.1 to 263.0, m/z 530.0 to 158.9 and m/z 591.8 to 493.9, respectively. Concentrations of GS-441524 and GS-443902 were determined using matrix-matched calibration curves prepared in blank liver or lung homogenates accordingly.

2.8. Metabolites identification

The CYP-related metabolites profiling was carried out using the LightSight® software (AB Sciex LLC, Toronto, Canada) with two information dependent acquisition (IDA) methods. For these two methods, the comprehensive MRM transitions sets of potential phase I metabolic biotransformation were predicted and generated by the LightSight® software based on two product ions of RDV, m/z 200.0 and 402.2, respectively. Two IDA methods in positive mode were then created using the corresponding predicted MRM transitions sets as survey scan and the enhanced product ion (EPI) scan as dependent scans with following IDA criteria: the two most intense peaks which exceeds 1000 cps after dynamic background subtraction of survey scan will be selected and subjected to EPI scans. Two samples, which represented the 0- and 5-min time points in HLMs stability assay, were injected into LC/MS/MS with a volume of 5 μL and analyzed by the IDA methods described above. Chromatographic separation of the parent RDV and metabolites was achieved on a Phenomenex Kinetex C18 column (50 mm × 2.1 mm, 2.6 μm). The two eluents were 0.1% formic acid in water (A) and 0.1% formic acid in acetonitrile (B). The mobile phase was delivered at a flow rate of 0.5 mL/min using a gradient of A and B as follows: from 0 to 4 min, 5% to 70% (v/v) B; from 4 to 5.8 min, 70% (v/v) B; from 5.8 to 6 min, 70% to 5% (v/v) B; from 6 to 10 min, 5% (v/v) B. Data obtained in the metabolites profiling was analyzed and processed using the LightSight® software.

3. Results

3.1. While substantial hydrolysis and extensive CYP-mediated metabolism render RDV unsuitable as an oral drug, the parent nucleoside GS-441524 exhibited favorable in vitro metabolic stability toward oral use

For oral administration, hepatic extraction is often the major barrier to the bioavailability of a drug. As a phosphoramidate prodrug, RDV is predicted to have high first pass hepatic extraction²¹. However, it is not clear if the extraction is due solely to the susceptibility of the phosphoramidate ester toward the abundant hydrolases in hepatocytes, or a combination of hydrolytic metabolism with CYP-mediated oxidative metabolism. On the other hand, the parent nucleoside GS-441524 is not susceptible to hydrolysis by the same hydrolases, and is not a substrate of major

CYP isozymes²⁸, though detailed hepatic clearance profile has not been fully characterized. Therefore, we first performed the routine *in vitro* liver microsomal assays to evaluate the impact of hepatic metabolism on RDV and GS-441524. The results are summarized in Table 1²¹. As expected, RDV showed very poor stability ($t_{1/2} = \sim 1$ min) in NADPH supplemented HLMs and MLMs, strongly suggesting that it may be subject to a complete hepatic extraction *in vivo*, and thus, may not be suitable for oral route of administration. Conversely, GS-441524 exhibited excellent stability with the remaining percentage determined to be over 91% at 60 min either in HLMs or MLMs (Fig. 2A), indicating that hepatic metabolism may not be a significant obstacle to its bioavailability following oral administration.

To gauge the impact of hydrolytic or non-NADPH dependent metabolism in the microsomal assays, RDV was also incubated in the liver microsomes without the CYP enzyme cofactor NADPH. While no significant change of $t_{1/2}$ in MLMs (1.0 min without NADPH versus 0.8 min with NADPH) was observed, the $t_{1/2}$ in HLMs was prolonged to 30.6 min from 1.1 min (Table 2). This suggests that CYP-mediated metabolism may be a key contributor to high RDV intrinsic clearance in HLMs, and along with the hydrolytic liability, may lead to excessive *in vivo* hepatic extraction of RDV in human.

Additionally, we also tested the stability of RDV and GS-441524 in CD-1 mouse plasma. Consistent with a previous report²⁴, RDV is highly susceptible in wild-type CD-1 mouse plasma. In our experiments, RDV became undetectable within seconds post addition, suggesting that the mice model is not appropriate for predicting RDV pharmacokinetics in human. It is known that carboxylesterases 1 and 2 are abundantly expressed in mice plasma, but not human³⁸. As anticipated, the parent nucleoside was stable in human or mice plasma with $t_{1/2}$ significantly greater than 24 h (Table 1).

3.2. CYP3A inhibitor cobicistat drastically enhanced RDV metabolic stability

Because CYP-mediated metabolism of RDV was shown to be a key contributor to its high intrinsic clearance in HLMs, we further investigated the potential of using a CYP inhibitor to enhance its stability against hepatic metabolism. For this purpose, we chose cobicistat (Cobi), an FDA-approved CYP3A inhibitor widely used in multiple combination therapies to boost the bioavailability of HIV-1 antiviral drugs. As shown in Fig. 2B, the addition of Cobi in the incubation completely inhibited CYP-mediated RDV metabolism, and drastically prolonged its $t_{1/2}$ in NADPH supplemented HLMs from 1.1 to 40.8 min (Table 2). In addition, Cobi did not

impact the hydrolytic (non-NADPH dependent) metabolism of RDV (Table 2, -NADPH). We also determined in HLMs the formation of the alanine metabolite (Ala-met), an intermediate metabolite formed during RDV hydrolytic activation. The results showed that CYP-mediated metabolism significantly decreased the conversion of RDV to the Ala-met intermediate (Fig. 2C). Interestingly, Cobi only partially restored the Ala-met level ($\sim 60\%$) at the end of incubation when compared to the results without the CYP enzyme cofactor NADPH (Fig. 2C), which was associated with a higher remaining percentage of intact RDV at 60 min (38.5% with NADPH/Cobi versus 26.1% without NADPH, Fig. 2B). This seems to indicate that Cobi can slow down the hydrolytic process of RDV in the presence of NADPH. Nevertheless, these results indicate that a combination treatment strategy with CYP3A inhibitor Cobi could mitigate the excessive CYP-mediated hepatic metabolism of RDV.

3.3. Metabolite profiling revealed that mono-oxidation is the major CYP-mediated metabolic pathway for RDV and the oxidation is likely on the phosphoramidate moiety but not the nucleoside core

To investigate the CYP-mediated metabolic pathway of RDV, we created two IDA methods to profile the potential CYP-related metabolites. The profiling was conducted by comparing two samples at 0 and 5 min from the microsomal assays in HLMs. The first IDA method, in which the survey scan was created based on a comprehensive predictive MRM (pMRM) transitions set of m/z 402.2, a product ion of RDV, detected only one related metabolite (M1) at the retention time of 4.31 min with a corresponding pMRM transition of m/z 619.2 to 418.2. M1 is the mono-oxidation metabolite (+16) of RDV (m/z 603.2). The second IDA method, in which the pMRM transitions was predicted using m/z 200.0, the most abundant product ions of RDV, detected a second metabolite (M2) at the retention time of 3.95 min in addition to the predominant mono-oxidation (M1) at 4.31 min (Fig. 3A). M2 has an m/z of 635.2 and is the di-oxidation metabolite (+32) of RDV (m/z 603.2). In the second IDA method, the mono- and di-oxidation metabolites were detected with the pMRM transitions of m/z 619.2 to 200.0 and m/z 635.2 to 200.0, respectively. These are consistent with the product ion spectrums obtained from the EPI dependent MS scans for m/z 619.2 (Fig. 3C) and 635.2 (Fig. 3D), where the m/z 402.1 observed with the parent RDV (Fig. 3B) disappeared. According to the product ion MS spectrum (Fig. 3B) and proposed fragmentation pathways (Supporting Information Fig. S1) of RDV, m/z 200.0 and 402.2 are likely generated by the breakage of the ribose ring, with m/z 200.0 representing the

Table 1 *In vitro* metabolic stabilities of RDV and GS-441524.

Compd.	Microsomal stability ^a				Plasma stability $t_{1/2}$ ^b	
	HLMs		MLMs		Human	Mouse
	$t_{1/2}$ ^b	CL _{int} ^c	$t_{1/2}$ ^b	CL _{int} ^c		
RDV	1.1 ± 0.1	1262.2 ± 68.6	0.8 ± 0.1	1683.8 ± 130.4	69 ²¹	<1
GS-441524	731.5 ± 54.4	1.9 ± 0.1	841.5 ± 210.0	1.7 ± 0.4	>1440	>1440

Data are presented as mean ± SD ($n \geq 2$).

^aCYP enzyme cofactor: NADPH.

^b $t_{1/2}$: half-life, min.

^cCL_{int}: intrinsic clearance, $\mu\text{L}/\text{min}/\text{mg}$ protein.

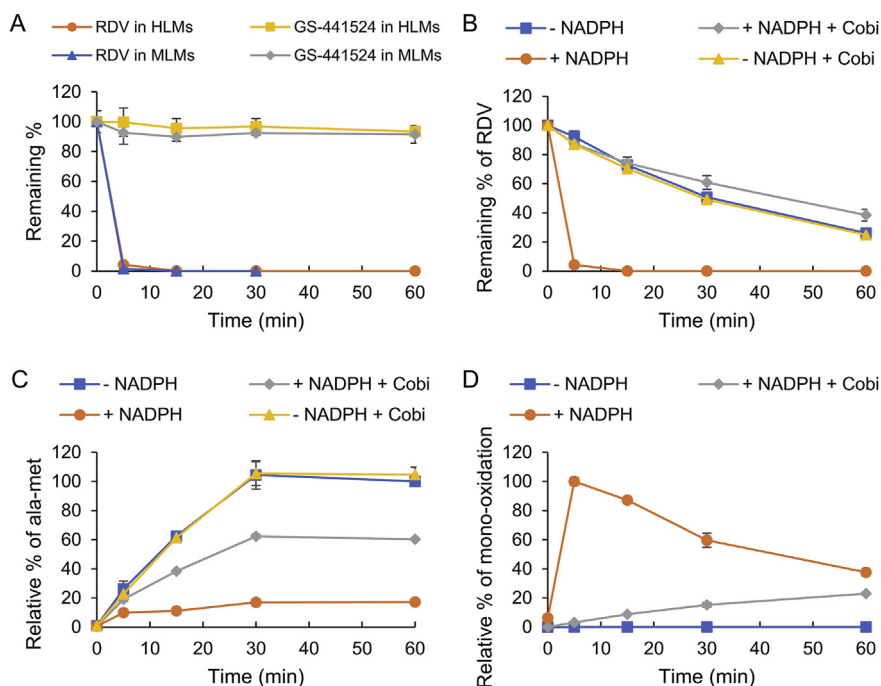


Figure 2 Microsomal stability of RDV and GS-441524. (A) Remaining percentage (%) of RDV or GS-441524 in HLMs and MLMs in the presence of cofactor NADPH. (B) Remaining percentage (%) of RDV in HLMs with or without cofactor NADPH and/or CYP3A inhibitor cobicistat (Cobi). (C) Relative percentage (% to the treatment without NADPH and Cobi at 60 min) of alanine metabolite (Ala-met) yielded by RDV in HLMs with or without cofactor NADPH and/or Cobi. (D) Relative percentage (% to the treatment with NADPH at 5 min) of mono-oxidized RDV yielded by RDV in HLMs with or without cofactor NADPH and/or Cobi. Data are presented as mean \pm SD ($n \geq 2$).

Table 2 RDV stability in HLMs with or without CYP3A inhibitor cobicistat (Cobi).

Compd.	HLMs stability $t_{1/2}$ (min)	
	-NADPH	+NADPH
RDV	30.6 \pm 1.6	1.1 \pm 0.1
RDV + Cobi	30.0 \pm 0.0	40.8 \pm 4.9

Data are presented as mean \pm SD ($n \geq 2$).

portion related to the nucleoside core, whereas m/z 402.2 representing the phosphoramidate ester moiety. Therefore, the mono- and di-oxidation metabolites were detected only with the product ions m/z 200.0 and 418.2 (mono-oxidation only), suggesting that the oxidation most likely occurs at the phosphoramidate ester moiety. This is also corroborated by the observed excellent stability of GS-441524 against CYP metabolism in HLMs. Since aromatic oxidation is one of the common CYP-mediated metabolisms, the principal mono-oxidation metabolite detected with RDV is likely *via* hydroxylation at the para position of the phenyl ring (Fig. 3E), presumably the most liable site to oxidative metabolism^{39,40}. The proposed fragmentation pathways of the mono-oxidation metabolite M1 are summarized in the Supporting Information Fig. S2. In addition, the mono-oxidation metabolite in the NADPH supplemented HLMs quickly reached the peak formation at 5 min (the earliest time point measured), followed by a gradual decrease with a $t_{1/2}$ of 38 min (Fig. 2D). Interestingly, the mono-oxidation metabolism appears to keep RDV from producing the Ala-met intermediate metabolite (Fig. 2C).

3.4. The parent nucleoside GS-441524 showed excellent bioavailability following oral administration, and produced significant levels of active triphosphate (GS-443902) in liver and lung tissue homogenates

RDV is subject to instant degradation in mouse plasma (Table 1), and thus, wild-type rodents, such as the CD-1 mice used herein, are not suitable for RDV pharmacokinetic studies. Therefore, despite the strong inhibition of Cobi on the CYP-mediated hepatic metabolism of RDV, we performed the *in vivo* pharmacokinetic assessment only for the parent nucleoside GS-441524. The oral bioavailability of GS-441524 was determined after an iv bolus of 5 mg/kg and an oral gavage of 10 mg/kg in CD-1 mice. The plasma concentrations of GS-441524 were quantified by LC/MS/MS method and the mean concentration *versus* time profile is shown in Fig. 4A. The main pharmacokinetic parameters of GS-441524 following iv and oral dosing are summarized in Table 3. After oral administration (10 mg/kg), GS-441524 appeared in the plasma at high levels ($>2 \mu\text{mol/L}$) from 0.25 to 2 h, and the C_{max} and T_{max} were determined to be 3.3 $\mu\text{mol/L}$ and 1 h, respectively. The terminal plasma $t_{1/2}$ was determined to be 2.5 h after iv bolus administration, and the mean residence time (MRT) was 4.2 h after oral administration. Significantly, GS-441524 showed a favorable oral bioavailability of 57% after normalizing the AUCs with the administered doses. The tissue distribution study was then carried out to further investigate its conversion to the active triphosphate GS-443902. In this study, GS-441524 was given to the CD-1 mice orally at a dose of 20 mg/kg, and both GS-441524 and the active triphosphate (GS-443902) were quantified in the

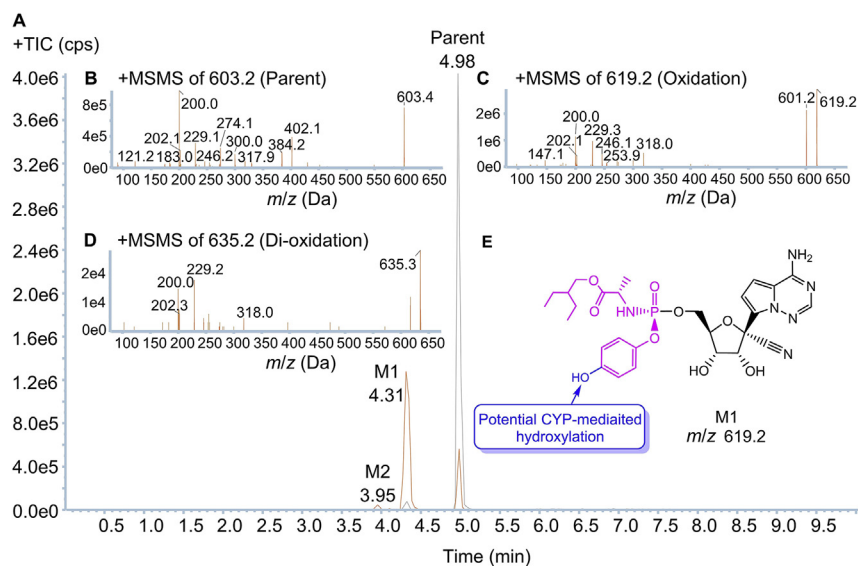


Figure 3 Chromatograms, product ion (MS/MS) spectrums and potential CYP-mediated metabolism of RDV and/or its mono-/di-oxidation metabolites identified in HLMs. (A) Total ion current (TIC) chromatograms of two samples from the NADPH supplemented HLMs incubation of RDV: 0 min (grey line) and 5 min (orange line). (B) Product ion spectrum of RDV (m/z 603.2). (C) Product ion spectrum of mono-oxidation metabolite M1 (m/z 619.2). (D) Product ion spectrum of di-oxidation metabolite M2 (m/z 635.2). (E) Potential structure of M1.

liver and lung homogenates at 1, 2, and 4 h post dosing. As shown in Fig. 4B, the parent nucleoside GS-441524 was extensively distributed into the liver and lung at levels higher than that in plasma during the first 4 h period. Importantly, the active triphosphate of the nucleoside was also detected and found to gradually accumulate in both liver and lung during this period. At 4 h post dosing, the active triphosphate concentrations in liver and lung were determined to be 0.63 and 0.1 $\mu\text{mol/L}$, corresponding to about 8% and 4% of the parent nucleoside in liver and lung, respectively.

4. Discussion

RDV is deemed unsuitable for oral administration when a systemic exposure or a targeting organ other than liver is required. This is mainly because the ProTide approach is typically intended for liver specific delivery by virtue of high hepatic extraction, as has been exemplified by two other FDA approved ProTide antivirals, sofosbuvir (SOF) and tenofovir alafenamide (TAF)^{41–43}. ProTide prodrugs are designed to deliver the nucleoside analogues into target cells as monophosphate to bypass the inefficient and typically rate-limiting step of nucleoside monophosphorylation^{44,45}. The activation of ProTide prodrugs generally involves hydrolases (carboxylesterases/cathepsin A) and phosphoramidases (histidine triad nucleotide binding proteins, HINTs) to release the monophosphorylated nucleotide^{21,41–45}. Because these enzymes are highly expressed in hepatocytes³⁴, preferential activation of the prodrugs occurs in the liver when given orally. However, the prodrugs can also accumulate in other organs with abundant hydrolases and HINTs expression such as GI tract and kidney. These might explain the common gastrointestinal side effects observed in patients with the orally SOF and TAF, and the less common adverse events related to liver and kidney damage including elevated liver enzymes and serum creatinine level,

which were also documented in COVID-19 patients treated with RDV^{28,46}. Interestingly, while SOF and TAF are oral antivirals for treating hepatitis C and hepatitis B virus, respectively, TAF is also used in combination therapies to treat HIV-1 which requires systemic exposure. TAF is only minimally metabolized by CYP3A4⁴⁷ and the primary hepatic metabolic route is *via* hydrolytic cleavage which apparently is significant but not prohibitive as indicated by a plasma oral bioavailability of 17% in dogs⁴³. By contrast, in our *in vitro* assessment, RDV was highly susceptible to CYP-mediated mono-oxidation. This, together with the hydrolytic metabolism, resulted in extremely low hepatic stability, suggesting that RDV is unsuitable for oral administration. However, the addition of Cobi fully restored the stability of RDV to the non-NADPH-dependent level in HLMs, demonstrating that a combination strategy with Cobi as a pharmacokinetic enhancer could mitigate the CYP-mediated metabolism, and the excessive hepatic extraction. Moreover, RDV is a substrate of P-glycoprotein (P-gp)^{28,37} and Cobi enhanced the oral bioavailability and plasma concentrations of TAF *via* inhibition on P-gp^{47,48}. Nevertheless, assessing the systemic drug exposure of the intact RDV following oral administration in a combination setting with Cobi requires *in vivo* pharmacokinetic studies which are not possible with the wild-type CD-1 mice due to its extraordinarily low plasma stability.

On the other hand, the potential of the parent nucleoside GS-441524 for COVID-19 treatment has been recognized and advocated³⁴. As aforementioned, RDV circulates predominantly as GS-441524 in the living systems, and GS-441524 has demonstrated exceptional efficacy in cats against feline coronavirus³⁴, comparable antiviral potency in cell-based settings against SARS-CoV-2²³, and higher conversion to the active triphosphate in Vero E6 cells²³ when compared to RDV. These findings strongly indicate that the role of the persisting GS-441524 metabolite in the clinical outcomes of RDV could be largely underestimated, which is corroborated by our *in vivo* studies. Notably, in our pharmacokinetic studies, GS-441524 exhibited a favorable oral bioavailability

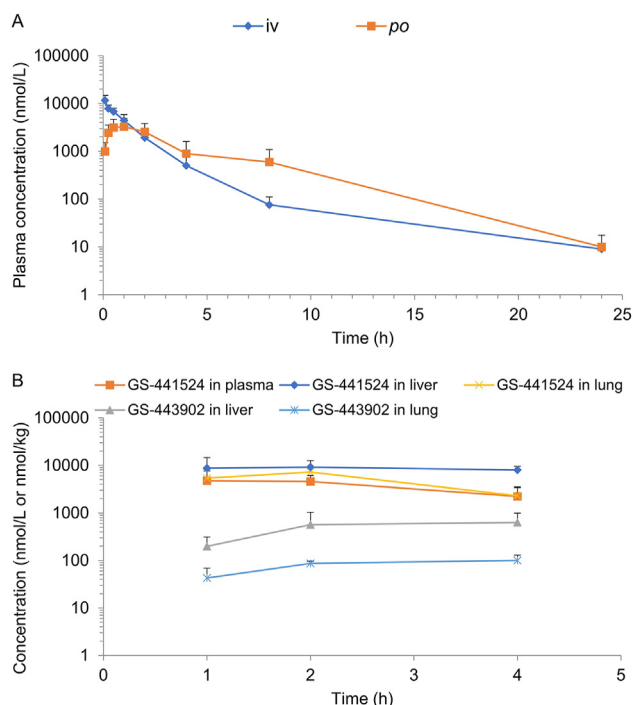


Figure 4 Pharmacokinetic profiles and tissue distribution of GS-441524. (A) Plasma concentration–time profiles of GS-441524 after iv (5 mg/kg, $n = 4$) and oral (*po*, 10 mg/kg, $n = 4$) administration. (B) Distribution of GS-441524 and its active triphosphate metabolite (GS-443902) to liver and lung at 1, 2, and 4 h after oral (20 mg/kg) administration, $n = 3$ per time point. Data are presented as mean \pm SD ($n \geq 3$).

($F = 57\%$) and a high level of plasma exposure in CD-1 mice. The subsequent tissue distribution studies also showed that the active triphosphate GS-443902 accumulated significantly in the mice liver (198–630 nmol/L) and lung (42.7–100 nmol/L) following an oral administration of GS-441524 (Fig. 4B). Specifically, GS-441524 in mice following a 20 mg/kg oral dose within the first 4 h resulted in concentrations in plasma or lung

($\geq 2.2 \mu\text{mol/L}$, Fig. 4B) well above its *in vitro* EC_{50} (0.62 $\mu\text{mol/L}$) or EC_{90} (1.34 $\mu\text{mol/L}$) against SARS-CoV-2 in Calu-3 2B4 human lung adenocarcinoma cells²³, Vero E6 cells ($\text{EC}_{50} = 0.47 \mu\text{mol/L}$, $\text{EC}_{90} = 0.71 \mu\text{mol/L}$)²³ or A549-hACE2 cells ($\text{EC}_{50} = 0.87 \mu\text{mol/L}$)⁴⁹. As for the tissue distribution of the triphosphate, although at a significantly lower level than in liver, the triphosphate accumulation in lung (42.7–100 nmol/L, Fig. 4B) appeared sufficient to produce potent antiviral activity when compared to the *in vitro* efficacy of RDV in primary human airway epithelial cells against SARS-CoV-2 ($\text{EC}_{50} = 10 \text{ nmol/L}$)²³. Being an adenosine analogue, GS-441524 is presumably phosphorylated by the intracellular adenosine kinase (ADK) at the initial rate-limiting step of its conversion to the triphosphate³⁴. ADK is highly conserved across mammalian species^{50,51} and is moderately expressed in many major organs in humans including liver and lung^{52,53}, suggesting that effective phosphorylation of GS-441524 is also expected in humans. In addition, GS-441524 has demonstrated good safety profile in cats^{31–33}, indicating that, if necessary, a potentially higher lung exposure of the active triphosphate can be achieved *via* a larger dose or multi-dose regimen of GS-441524. In short, the results of our research indicate that RDV nucleoside GS-441524 could be a viable oral drug, and support further studies in humans to examine its clinical efficacy as an oral drug against SARS-CoV-2.

5. Conclusions

In this study, we have performed an *in vitro* and *in vivo* DMPK assessment to evaluate the potential of RDV and its parent nucleoside GS-441524 as oral antiviral drugs. While the *in vitro* metabolic assessments in HLMs confirmed that RDV alone is unsuitable for oral administration, a combination with Cobi could inhibit the CYP-mediated metabolism and potentially mitigate the hepatic extraction *via* oral route. A metabolite profiling assay also revealed that the major CYP-mediated metabolic pathway of RDV is a mono-oxidation likely on the phosphoramidate moiety but not the nucleoside core. Importantly, in pharmacokinetic studies in CD-1 mice, the parent nucleoside GS-441524 exhibited favorable oral bioavailability and seemingly adequate intracellular conversion into the nucleoside triphosphate, supporting further human efficacy studies on GS-441524 as an oral drug for treating COVID-19.

Acknowledgments

We thank the Center for Drug Design, College of Pharmacy, University of Minnesota, USA, for supporting this research.

Author contributions

Jiashu Xie and Zhengqiang Wang conceptualized the research. Jiashu Xie designed and performed the *in vitro* and *in vivo* DMPK studies. Jiashu Xie and Zhengqiang Wang wrote the manuscript. Both authors have read and agreed to the published version of the manuscript.

Conflicts of interest

The authors declare no conflict of interest.

Table 3 Pharmacokinetic parameters of GS-441524 after iv and oral administration.

Parameters	iv (5 mg/kg, $n = 4$)	<i>po</i> (10 mg/kg, $n = 4$)
$t_{1/2}$ (h)	2.5	2.9
T_{max} (h)	0.083	1.0
C_{max} (nmol/L)	11,619.3	3281.0
AUC_{0-t} (h·nmol/L)	14,763.2	16,795.0
$\text{AUC}_{0-\infty}$ (h·nmol/L)	14,795.5	16,836.3
MRT_{0-t} (h)	1.7	4.2
V (L/kg)	4.2	8.4
CL (L/h/kg)	1.2	2.0

$t_{1/2}$, terminal half-life. T_{max} , time to reach C_{max} . C_{max} , maximum plasma concentration. AUC_{0-t} , area under the concentration–time curve from the time of dosing to the last quantifiable time point. $\text{AUC}_{0-\infty}$, area under the concentration–time curve from the time of dosing to infinity. MRT , mean residence time. V , volume of distribution. CL , clearance.

Appendix A. Supporting information

Supporting information to this article can be found online at <https://doi.org/10.1016/j.apsb.2021.03.028>.

References

- World Health Organization. WHO coronavirus disease (COVID-19) dashboard. Available from: <https://covid19.who.int/>; 2020.
- V Kovski P, Kratzel A, Steiner S, Stalder H, Thiel V. Coronavirus biology and replication: implications for SARS-CoV-2. *Nat Rev Microbiol* 2021;**19**:155–70.
- Billah MA, Miah MM, Khan MN. Reproductive number of coronavirus: a systematic review and meta-analysis based on global level evidence. *PLoS One* 2020;**15**:e0242128.
- Sanche S, Lin YT, Xu C, Romero-Severson E, Hengartner N, Ke R. High contagiousness and rapid spread of severe acute respiratory syndrome coronavirus 2. *Emerg Infect Dis* 2020;**26**:1470–7.
- The Lancet Respiratory Medicine. COVID-19 transmission-up in the air. *Lancet Respir Med* 2020;**8**:1159.
- Harrison AG, Lin T, Wang P. Mechanisms of SARS-CoV-2 transmission and pathogenesis. *Trends Immunol* 2020;**41**:1100–15.
- Arons MM, Hatfield KM, Reddy SC, Kimball A, James A, Jacobs JR, et al. Presymptomatic SARS-CoV-2 infections and transmission in a skilled nursing facility. *N Engl J Med* 2020;**382**:2081–90.
- Pan X, Chen D, Xia Y, Wu X, Li T, Ou X, et al. Asymptomatic cases in a family cluster with SARS-CoV-2 infection. *Lancet Infect Dis* 2020;**20**:410–1.
- Rothe C, Schunk M, Sothmann P, Bretzel G, Froeschl G, Wallrauch C, et al. Transmission of 2019-nCoV infection from an asymptomatic contact in Germany. *N Engl J Med* 2020;**382**:970–1.
- Li R, Pei S, Chen B, Song Y, Zhang T, Yang W, et al. Substantial undocumented infection facilitates the rapid dissemination of novel coronavirus (SARS-CoV-2). *Science* 2020;**368**:489–93.
- Cevik M, Kuppalli K, Kindrachuk J, Peiris M. Virology, transmission, and pathogenesis of SARS-CoV-2. *BMJ* 2020;**371**:m3862.
- Mason RJ. Pathogenesis of COVID-19 from a cell biology perspective. *Eur Respir J* 2020;**55**:2000607.
- Hu B, Guo H, Zhou P, Shi ZL. Characteristics of SARS-CoV-2 and COVID-19. *Nat Rev Microbiol* 2021;**19**:141–54.
- Zou L, Ruan F, Huang M, Liang L, Huang H, Hong Z, et al. SARS-CoV-2 viral load in upper respiratory specimens of infected patients. *N Engl J Med* 2020;**382**:1177–9.
- Wolfel R, Corman VM, Guggemos W, Seilmaier M, Zange S, Muller MA, et al. Virological assessment of hospitalized patients with COVID-2019. *Nature* 2020;**581**:465–9.
- Fajnzylber J, Regan J, Coxen K, Corry H, Wong C, Rosenthal A, et al. SARS-CoV-2 viral load is associated with increased disease severity and mortality. *Nat Commun* 2020;**11**:5493.
- Cox RM, Wolf JD, Plemper RK. Therapeutically administered ribonucleoside analogue MK-4482/EIDD-2801 blocks SARS-CoV-2 transmission in ferrets. *Nat Microbiol* 2021;**6**:11–8.
- Rubin D, Chan-Tack K, Farley J, Sherwat A. FDA approval of Remdesivir—a step in the right direction. *N Engl J Med* 2020;**383**:2598–600.
- Warren TK, Jordan R, Lo MK, Ray AS, Mackman RL, Soloveva V, et al. Therapeutic efficacy of the small molecule GS-5734 against Ebola virus in rhesus monkeys. *Nature* 2016;**531**:381–5.
- Cho A, Saunders OL, Butler T, Zhang L, Xu J, Vela JE, et al. Synthesis and antiviral activity of a series of 1'-substituted 4-aza-7,9-dideazaadenosine C-nucleosides. *Bioorg Med Chem Lett* 2012;**22**:2705–7.
- Siegel D, Hui HC, Doerffler E, Clarke MO, Chun K, Zhang L, et al. Discovery and synthesis of a phosphoramidate prodrug of a pyrrolo [2,1-f][triazin-4-amino] adenine C-nucleoside (GS-5734) for the treatment of Ebola and emerging viruses. *J Med Chem* 2017;**60**:1648–61.
- Lo MK, Jordan R, Arvey A, Sudhamsu J, Shrivastava-Ranjan P, Hotard AL, et al. GS-5734 and its parent nucleoside analog inhibit filo-, pneumo-, and paramyxoviruses. *Sci Rep* 2017;**7**:43395.
- Pruijssers AJ, George AS, Schafer A, Leist SR, Gralinski LE, Dinnon 3rd KH, et al. Remdesivir inhibits SARS-CoV-2 in human lung cells and chimeric SARS-CoV expressing the SARS-CoV-2 RNA polymerase in mice. *Cell Rep* 2020;**32**:107940.
- Sheahan TP, Sims AC, Graham RL, Menachery VD, Gralinski LE, Case JB, et al. Broad-spectrum antiviral GS-5734 inhibits both epidemic and zoonotic coronaviruses. *Sci Transl Med* 2017;**9**:eaal3653.
- Sheahan TP, Sims AC, Leist SR, Schafer A, Won J, Brown AJ, et al. Comparative therapeutic efficacy of remdesivir and combination lopinavir, ritonavir, and interferon beta against MERS-CoV. *Nat Commun* 2020;**11**:222.
- Wang M, Cao R, Zhang L, Yang X, Liu J, Xu M, et al. Remdesivir and chloroquine effectively inhibit the recently emerged novel coronavirus (2019-nCoV) *in vitro*. *Cell Res* 2020;**30**:269–71.
- Agostini ML, Andres EL, Sims AC, Graham RL, Sheahan TP, Lu X, et al. Coronavirus susceptibility to the antiviral Remdesivir (GS-5734) is mediated by the viral polymerase and the proofreading exoribonuclease. *mBio* 2018;**9**:e00221-18.
- U.S. Food and Drug Administration. Veklury (remdesivir) EUA fact sheet for healthcare providers. Available from: <https://www.fda.gov/media/137566/download>; 2020.
- Gordon CJ, Tchesnokov EP, Woolner E, Perry JK, Feng JY, Porter DP, et al. Remdesivir is a direct-acting antiviral that inhibits RNA-dependent RNA polymerase from severe acute respiratory syndrome coronavirus 2 with high potency. *J Biol Chem* 2020;**295**:6785–97.
- Humeniuk R, Mathias A, Cao H, Osinusi A, Shen G, Chng E, et al. Safety, tolerability, and pharmacokinetics of Remdesivir, an antiviral for treatment of COVID-19, in healthy subjects. *Clin Transl Sci* 2020;**13**:896–906.
- Pedersen NC, Perron M, Bannasch M, Montgomery E, Murakami E, Liepnieks M, et al. Efficacy and safety of the nucleoside analog GS-441524 for treatment of cats with naturally occurring feline infectious peritonitis. *J Feline Med Surg* 2019;**21**:271–81.
- Dickinson PJ, Bannasch M, Thomasy SM, Murthy VD, Vernau KM, Liepnieks M, et al. Antiviral treatment using the adenosine nucleoside analogue GS-441524 in cats with clinically diagnosed neurological feline infectious peritonitis. *J Vet Intern Med* 2020;**34**:1587–93.
- Murphy BG, Perron M, Murakami E, Bauer K, Park Y, Eckstrand C, et al. The nucleoside analog GS-441524 strongly inhibits feline infectious peritonitis (FIP) virus in tissue culture and experimental cat infection studies. *Vet Microbiol* 2018;**219**:226–33.
- Yan VC, Muller FL. Advantages of the parent nucleoside GS-441524 over Remdesivir for COVID-19 treatment. *ACS Med Chem Lett* 2020;**11**:1361–6.
- Williamson BN, Feldmann F, Schwarz B, Meade-White K, Porter DP, Schulz J, et al. Clinical benefit of remdesivir in rhesus macaques infected with SARS-CoV-2. *Nature* 2020;**585**:273–6.
- Hu WJ, Chang L, Yang Y, Wang X, Xie YC, Shen JS, et al. Pharmacokinetics and tissue distribution of remdesivir and its metabolites nucleotide monophosphate, nucleotide triphosphate, and nucleoside in mice. *Acta Pharmacol Sin* 2020. Available from: <https://www.nature.com/articles/s41401-020-00537-9>.
- Aleissa MM, Silverman EA, Paredes Acosta LM, Nutt CT, Richterman A, Marty FM. New perspectives on antimicrobial agents: remdesivir treatment for COVID-19. *Antimicrob Agents Chemother* 2020;**65**:1814–20.
- Li B, Sedlacek M, Manoharan I, Boopathy R, Duysen EG, Masson P, et al. Butyrylcholinesterase, paraoxonase, and albumin esterase, but not carboxylesterase, are present in human plasma. *Biochem Pharmacol* 2005;**70**:1673–84.
- Bathelt CM, Ridder L, Mulholland AJ, Harvey JN. Aromatic hydroxylation by cytochrome P450: model calculations of mechanism and substituent effects. *J Am Chem Soc* 2003;**125**:15004–5.

40. Sheridan RP, Korzekwa KR, Torres RA, Walker MJ. Empirical regioselectivity models for human cytochromes P450 3A4, 2D6, and 2C9. *J Med Chem* 2007;**50**:3173–84.
41. Kirby BJ, Symonds WT, Kearney BP, Mathias AA. Pharmacokinetic, pharmacodynamic, and drug-interaction profile of the hepatitis C Virus NS5B polymerase inhibitor Sofosbuvir. *Clin Pharmacokinet* 2015;**54**:677–90.
42. Sofia MJ, Bao D, Chang W, Du J, Nagarathnam D, Rachakonda S, et al. Discovery of a beta-d-2'-deoxy-2'-alpha-fluoro-2'-beta-C-methyluridine nucleotide prodrug (PSI-7977) for the treatment of hepatitis C virus. *J Med Chem* 2010;**53**:7202–18.
43. Lee WA, He GX, Eisenberg E, Cihlar T, Swaminathan S, Mulato A, et al. Selective intracellular activation of a novel prodrug of the human immunodeficiency virus reverse transcriptase inhibitor tenofovir leads to preferential distribution and accumulation in lymphatic tissue. *Antimicrob Agents Chemother* 2005;**49**:1898–906.
44. Mehellou Y, Rattan HS, Balzarini J. The ProTide prodrug technology: from the concept to the clinic. *J Med Chem* 2018;**61**:2211–26.
45. Wiemer AJ. Metabolic efficacy of phosphate prodrugs and the Remdesivir paradigm. *ACS Pharmacol Transl Sci* 2020;**3**:613–26.
46. Beigel JH, Tomashek KM, Dodd LE, Mehta AK, Zingman BS, Kalil AC, et al. Remdesivir for the treatment of Covid-19—final report. *N Engl J Med* 2020;**383**:1813–26.
47. Yamada H, Yonemura T, Nemoto T, Ninomiya N, Irie S. Pharmacokinetics of tenofovir alafenamide, tenofovir, and emtricitabine following administration of coformulated emtricitabine/tenofovir alafenamide in healthy Japanese subjects. *Clin Pharmacol Drug Dev* 2019;**8**:511–20.
48. Lepist EI, Phan TK, Roy A, Tong L, MacLennan K, Murray B, et al. Cobicistat boosts the intestinal absorption of transport substrates, including HIV protease inhibitors and GS-7340, *in vitro*. *Antimicrob Agents Chemother* 2012;**56**:5409–13.
49. Xie X, Muruato AE, Zhang X, Lokugamage KG, Fontes-Garfias CR, Zou J, et al. A nanoluciferase SARS-CoV-2 for rapid neutralization testing and screening of anti-infective drugs for COVID-19. *Nat Commun* 2020;**11**:5214.
50. Park J, Gupta RS. Adenosine kinase and ribokinase—the RK family of proteins. *Cell Mol Life Sci* 2008;**65**:2875–96.
51. Kiese K, Jablonski J, Boison D, Kobow K. Dynamic regulation of the adenosine kinase gene during early postnatal brain development and maturation. *Front Mol Neurosci* 2016;**9**:99.
52. Uhlen M, Fagerberg L, Hallstrom BM, Lindskog C, Oksvold P, Mardinoglu A, et al. Proteomics. Tissue-based map of the human proteome. *Science* 2015;**347**:1260419.
53. Adenosine Kinase. Human protein atlas (version 20.1). Available from: <http://www.proteinatlas.org>.